Photoacoustics 33 (2023) 100553

Contents lists available at ScienceDirect

Photoacoustics

journal homepage: www.elsevier.com/locate/pacs

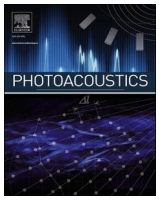

Light-induced thermoelastic sensor for ppb-level H_2S detection in a SF_6 gas matrices exploiting a mini-multi-pass cell and quartz tuning fork photodetector

Bo Sun [a,b], Pietro Patimisco [b], Angelo Sampaolo [b], Andrea Zifarelli [b], Vincenzo Spagnolo [a,b,*], Hongpeng Wu [a,b,*], Lei Dong [a,b,*]

[a] Laboratory of Quantum Optics and Quantum Optics Devices, Institute of Laser Spectroscopy, Shanxi University, Taiyuan 030006, China
[b] PolySense Lab-Dipartimento Interateneo di Fisica, University and Politecnico of Bari, Via Amendola 173, Bari, Italy

ARTICLE INFO

Keywords:
Light-induced thermoelastic spectroscopy
Quartz tuning fork
H_2S detection
Sulphur hexafluoride

ABSTRACT

We present an optical sensor based on light-induced thermoelastic spectroscopy for the detection of hydrogen sulfide (H_2S) in sulfur hexafluoride (SF_6). The sensor incorporates a compact multi-pass cell measuring 6 cm × 4 cm × 4 cm and utilizes a quartz tuning fork (QTF) photodetector. A 1.58 μm near-infrared distributed feedback (DFB) laser with an optical power of 30 mW serves as the excitation source. The sensor achieved a minimum detection limit (MDL) of ~300 ppb at an integration time of 300 ms, corresponding to a normalized noise equivalent absorption coefficient (NNEA) of 3.96×10^{-9} W·cm^{-1}·Hz$^{-1/2}$. By extending the integration time to 100 s, the MDL can be reduced to ~25 ppb. The sensor exhibits a response time of ~1 min for a gas flow rate of 70 sccm.

1. Introduction

Sulfur hexafluoride (SF_6) is a colorless, odorless, non-toxic, non-flammable chemically inert gas. It possesses excellent dielectric properties, making it an exceptional arc-quenching medium. When compared to air, SF_6 exhibits a significantly higher arc-extinguishing ability, being 100 times more effective. Moreover, SF_6 demonstrates superior insulation capability, which is 2.5 times better than that of air, along with a density that is 5.6 times greater. Consequently, SF_6 has emerged as a replacement for oil and compressed air as an insulation medium in power grid systems. Applications of SF_6 include gas-insulated switchgears, transmission pipes, gas circuit breakers, and transformers [1–3]. In power grid, gas-insulated switchgears (GIS) play a crucial role in facilitating high-voltage switch on/off operations exceeding 1 MV [4]. Nevertheless, over prolonged periods of operation, corona, partial discharge, and spark discharge may transpire within the GIS. SF_6 is typically stable under normal conditions. However, in the presence of metals within an overheated environment, discharge events can lead to the generation of various decomposition compounds [5,6], such as SF_4, SF_3, SF_2, and S_2F_{10}. These low-fluorine sulfides have the potential to react with minute amounts of air and moisture present within the equipment, resulting in the formation of toxic and corrosive compounds, such as H_2S, HF, SOF_2, SO_2F_2, SOF_4, SO_2 and CO [7–10]. Monitoring the concentrations and formation rates of these decomposition products can provide insights into the type and progression of internal faults within the equipment [11]. The detection of hydrogen sulfide (H_2S) traces holds particular significance in assessing the discharge energy of a fault and determining whether the fault involves solid insulation materials [12]. Therefore, achieving detection sensitivity in the sub ppm-range for H_2S in SF_6 becomes crucial for ensuring the security maintenance of the power grid [13].

In recent years, various techniques have been employed for the detection of decomposition compounds formed within the SF_6 matrix. These techniques include tube detection, metal-oxide semiconductor sensing, gas chromatography [14–16] and, more recently, in situ and real-time optical sensors [17,18]. In 2017, the first demonstration of a photoacoustic spectroscopy (PAS) sensor for H_2S detection in SF_6 was conducted [13]. PAS employs a microphone to detect the faint sound waves produced as a result of molecule absorption through the photoacoustic effect. However, the use of a highly sensitive microphone with a

* Corresponding authors at: Laboratory of Quantum Optics and Quantum Optics Devices, Institute of Laser Spectroscopy, Shanxi University, Taiyuan 030006, China.
E-mail addresses: vincenzoluigi.spagnolo@poliba.it (V. Spagnolo), wuhp@sxu.edu.cn (H. Wu), donglei@sxu.edu.cn (L. Dong).

https://doi.org/10.1016/j.pacs.2023.100553
Received 12 July 2023; Received in revised form 29 August 2023; Accepted 29 August 2023
Available online 31 August 2023

wide acoustic detection bandwidth presents a challenge when installing a PAS sensor in a noisy environment, as any external acoustic source can contribute to the overall signal. As a variant of PAS, quartz enhanced photoacoustic spectroscopy (QEPAS) is particularly well-suited for in situ and real-time measurement applications owing to its robust immunity to environmental noise [19]. This is achieved by utilizing a quartz tuning fork (QTF) in place of the traditional microphone for sound wave detection. The QTF operates at resonant frequencies with a narrow bandwidth (<1 Hz), effectively filtering out any noise contributions outside of this range and ensuring high immunity to environmental noise. In QEPAS, the quartz tuning fork (QTF) is completely immersed in the fluid containing the target molecules that need to be detected. However, this immersion poses limitations on the application of QEPAS techniques for the detection of decomposition compounds within the SF_6 matrix for two primary reasons. First, the heavy molecular weight of SF_6 molecules results in significant damping of the vibration amplitudes of the QTF within the SF_6-based matrix, as compared to the behavior observed in standard air [20]. Second, decomposition substances such as SO_2 and H_2S in SF_6 exhibit high corrosiveness, particularly towards the metal electrodes coated on the surfaces of the QTF. Consequently, this presents a constraint on the long-term operation of the QEPAS system. [21,22].

Recently, QTFs have been proposed as a sensitive and cost-effective alternative to infrared photodetectors in optical sensors that utilize light-induced thermoelastic spectroscopy (LITES) [23–27]. The LITES setup architecture closely resembles that of tunable diode laser spectroscopy combined with the wavelength modulation technique. In this setup, an intensity-modulated laser beam traverses a gas cell, and subsequently, the light emerging from the gas cell is focused onto one of the prongs of the QTF, inducing localized modulated heating. This thermal energy generates a local strain field, which in turns give rises to a piezoelectric charge distribution. Similar to QEPAS, this charge distribution can be collected using the metal contact patterns deposited on the surface of the QTF. Thus, both QEPAS and LITES utilize the properties of the QTF, such as the high resonance Q-factor, narrow frequency bandwidth, wavelength independence, and the possibility of implementing a wavelength modulation approach with second harmonic detection to achieve a noise-free background [24]. The main difference between QEPAS and LITES lies in the physical phenomenon that causes the oscillation of the QTF prongs and consequently the production of an electric charge distribution. In contrast to QEPAS, LITES offers the distinct advantage of having the QTF located outside the gas cell, enabling non-contact measurements [25–32].

Here we report on the implementation of a LITES sensor for detecting H_2S in SF_6 in order to monitor gas-insulated switchgears. The vibrational characteristics of a standard 32 kHz-QTF are analyzed in different environments (SF_6 and N_2), validating the benefits of employing LITES technology compared to QEPAS for SF_6 decomposition monitoring. The operating parameters of the developed LITES sensor are optimized, and the obtained results are thoroughly discussed.

2. Vibration analysis of QTF in N_2 and SF_6 environments

The QTF is a mechanically forked structure composed of a quartz crystal with piezoelectric properties. When it absorbs energy from sound waves or a modulated laser beam that resonates with the frequency of the QTF, the prongs of the fork initiate vibration, resulting in the generation of a strain field. Utilizing the piezoelectric effect, a charge distribution is produced and collected through the electrode pattern distributed on the surface of the prongs. This electrical signal can be demodulated using a lock-in amplifier, allowing for the extraction of a signal that is directly proportional to the intensities of the sound waves (QEPAS) or the absorbed laser beam (LITES).

The resonant frequency of the QTF is determined by the prongs geometry, and the resonant frequency can be estimated by the following equation [32]:

$$f = \frac{1}{2\pi}\sqrt{\frac{k}{m_{eff}}} \approx 1.015\frac{w}{2\pi L^2}\sqrt{\frac{E}{\rho}} \tag{1}$$

where $k = Etw^3/(4L^3)$ is stiffness, $m_{eff} = 0.2427\rho Lwt$ is effective mass, E and ρ are Young's modulus and density of quartz, respectively, *L, w, t* are the prongs length, width, and thickness, respectively. *L, w, t* for a commercial standard 32-kHz QTF were measured to be 3.8 mm, 1.4 mm and 0.3 mm, respectively. For certain gases with low relaxation rates such as methane, carbon monoxide, and nitric oxide, the frequency of a standard 32-kHz QTF may not satisfy the requirement $\tau \ll 1/f$ (τ is molecular vibration-rotational relaxation rate) needed for effective generation of electrical signals. However, when measuring H_2S concentration, which is a fast-relaxing molecule, the 32-kHz QTF can be operated successfully [33]. In addition to its small size, the standard 32-kHz QTF offers several advantages including affordability, low signal loss, wide dynamic range, robustness against environmental noise, and high temperature resistance [34–37]. Nonetheless, its applicability for detecting SF_6 decomposition may be limited due to the high density of SF_6 in comparison to standard air or N_2.

When a QTF undergoes small amplitude harmonic oscillations while immersed in a fluid medium, it induces movement in the surrounding fluid. This phenomenon leads to energy dissipation through acoustic losses and introduces additional inertia. As a result, the reaction force comprises a resistive component responsible for energy dissipation and a reactive component that contributes to the increased inertia experienced by the vibrating QTF. Consequently, the vibration of a QTF's prong can be described by a fourth-order differential equation under these conditions. [32]:

$$EI\frac{\partial^4 y}{\partial x^4}(x,t) + C_d\frac{\partial y}{\partial t}(x,t) + (\rho A + u)\frac{\partial^4 y}{\partial t^4}(x,t) = 0 \tag{2}$$

where ρ represents the density of the quartz material, E stands for the Young's modulus of the material, t denotes time, C_d is the damping parameter, u is the added mass per unit length, A is defined as the cross product of the crystal thickness w and the prong width T, and the directions x and y refer to the plane of the QTF. For small damping, it has been demonstrated that the presence of an added mass causes a red shift Δf in the resonance frequency of the QTF [34], in comparison to its resonance frequency in a vacuum:

$$\Delta f = -\frac{1}{2}\frac{u}{\rho A} \tag{3}$$

The added mass is directly proportional to the density ρ_0 of the gas medium and, consequently, its pressure. Thereby when operating the QTF in SF_6 compared to N_2 or standard air, larger red shifts are expected.

The Q-factor of a resonance mode is a measure of the energy loss experienced by the prongs while vibrating. To model the damping effect caused by air, an analytical expression derived by Hosaka et al. [38] can be utilized, allowing for the formulation of the contribution of gas damping to the Q-factor:

$$Q_{gas} \approx \frac{4\rho T w^2 f}{3\mu w + \frac{3}{4}w^2\sqrt{4\pi\rho_0\mu f}} \tag{4}$$

where μ is the gas viscosity. Gas damping has been identified as the primary mechanism responsible for energy loss, both in the case of N_2 and SF_6 [20]. The density of N_2 and SF_6 are 1.16 kg/m^3 and 6.52 kg/m^3 [15], thereby, a lower QTF Q-factor is expected when it is placed in a SF_6 matrix with respect to N_2 or standard air. To evaluate the decrease in the Q-factor of a 32 kHz QTF when operated in SF_6 compared to N_2, the experimental arrangement illustrated in Fig. 1(a) was utilized. A high-resolution function generator was utilized to generate a sine voltage spanning the frequency range of 32760–32770 Hz for exciting the QTF. The current output from QTF was converted to voltage through an operational amplifier and subsequently demodulated using a lock-in

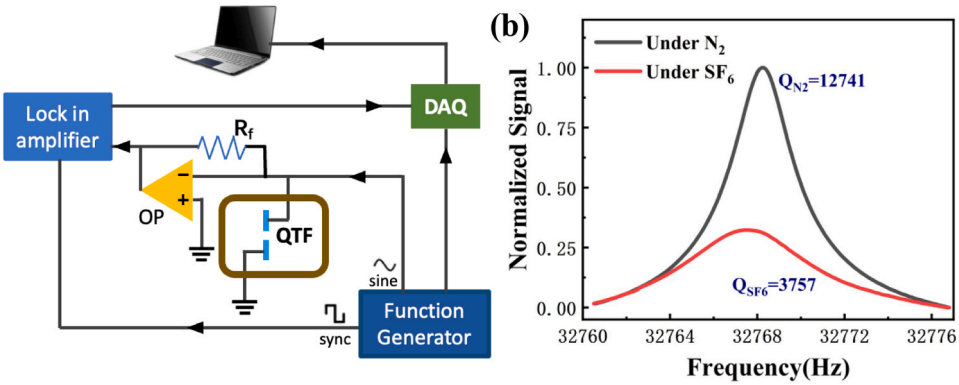

Fig. 1. (a) schematic of the setup used for QTF frequency scanning. OP: operational amplifier, DAQ: data acquisition, feedback resistor: Rf= 10 MΩ. (b) Frequency response curves of the 32 kHz-QTF at atmospheric pressure in N_2 and SF_6.

amplifier (Stanford Research Model SR830). The lock-in amplifier was configured with parameters including a filter slope of 12 dB/oct and a time constant of 100 ms, resulting in a detection bandwidth of 1.6675 Hz. During the measurements, an integration time of 300 ms was employed. The resonance curves of a 32 kHz-QTF immersed in SF_6 or N_2 at atmospheric pressure are displayed in Fig. 1(b). The QTF signal at the resonance frequency in SF_6 is 3.2 times smaller than that in N_2, the quality factor drops from 12741 to 3757, and, as expected, the resonance frequency red shifts.

3. LITES H_2S detector in SF_6 setup

In contrast to QEPAS, the LITES technique offers a non-contact sensing approach with comparable sensitivity levels [39–41]. A scheme of the configuration of a standard QEPAS and LITES technique is reported in Fig. 2(a) and (b), respectively.

In the LITES technique, the QTF operates as an infrared photodetector, offering a cost-effective alternative to expensive photodetectors while eliminating the need for thermoelectric cooling systems [40]. A schematic of the complete architecture of the LITES sensor for H_2S detection in a SF_6 matrix is depicted in Fig. 3. For the excitation source, a low-cost distributed feedback (DFB) pigtailed laser (FITEL, model FRL 15DCWD-A82), emitting within the range 1563–1583 nm, was employed. The laser is securely mounted on the driver board and controlled by a computer to maintain a stable temperature and set the laser current. The DFB laser targets a specific H_2S absorption peak occurring at 6320.55 cm^{-1}. Despite the low line strength of the targeted H_2S absorption feature, which measures 1.1×10^{-22} cm/mol, no fiber amplifier was utilized in contrast to previous experiments [15,33]. This simplifies the setup architecture, reduces the overall cost, and minimizes the size of the sensor system. A function generator is used to modulate the laser current at the half of the QTF's fundamental frequency. The function generator is additionally responsible for supplying a voltage ramp to the laser, allowing for a gradual scanning of the laser wavelength across the desired absorption feature. The fiber output beam is then coupled with a non-commercial mini multi-pass cell (MMPC) that contains the target gas sample. The MMPC consists of two spherical mirrors and is designed to generate a spot pattern with 7-nonintersecting-circle [18]. Within the MMPC, the laser beam undergoes over a hundred reflections between two high-reflection mirrors. Subsequently, it exits through an aperture in the output mirror and illuminates the QTF near to one of the prongs base, precisely at 3.8 mm from the QTF's prong top, where the strongest LITES signal is predicted [30,42]. The QTF signal is then directed to a low-impedance amplifier with a feedback resistor of 10 MΩ. Its output signal is subsequently fed into a lock-in amplifier (Stanford Research Systems, Model SR830) for the demodulation at the QTF resonance frequency, utilizing wavelength modulation and second harmonic detection. The lock-in amplifier parameters employed include a filter slope of 12 dB/oct, a time constant of 100 ms, and an integration time of 300 ms, which are consistent with previous experiments.

The MMPC is positioned within a chamber that equipped with a pre-aligned fiber collimator and a fiber connector (see Fig. 3). These components facilitate the coupling of the pigtail laser on one side and enable the laser beam to exit through a quartz window with a diameter of 1 cm on the opposite side. To regulate the pressure inside the chamber and the gas flow, a pressure meter and a flux meter are employed. To generate various concentrations of H_2S in SF_6, a gas mixing system is utilized, starting from two certified standard cylinders containing pure SF_6 and SF_6 with a concentration of 100 ppm H_2S. These gas mixtures are then introduced into the MMPC chamber for sensor analysis, testing, and calibration purposes. Within the experimental setup, the QTF is housed in a small cell with a volume of 6 cm^3, featuring an optical window. This cell is connected to a diaphragm pump and a pressure meter via a needle valve, allowing for the adjustment and monitoring of the QTF's operating pressure.

Compared to the traditional LITES technology that utilizes a gas cell as absorption path [23], the MMPC enables the achievement of a

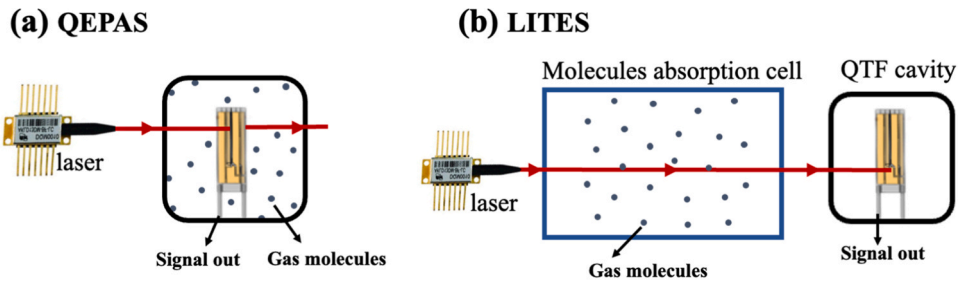

Fig. 2. (a) Sketch of a standard QEPAS technique. The QTF is immersed in the gas cell. (b) Sketch of a standard LITES technique. The QTF operates as an infrared photodetector outside of the gas cell.

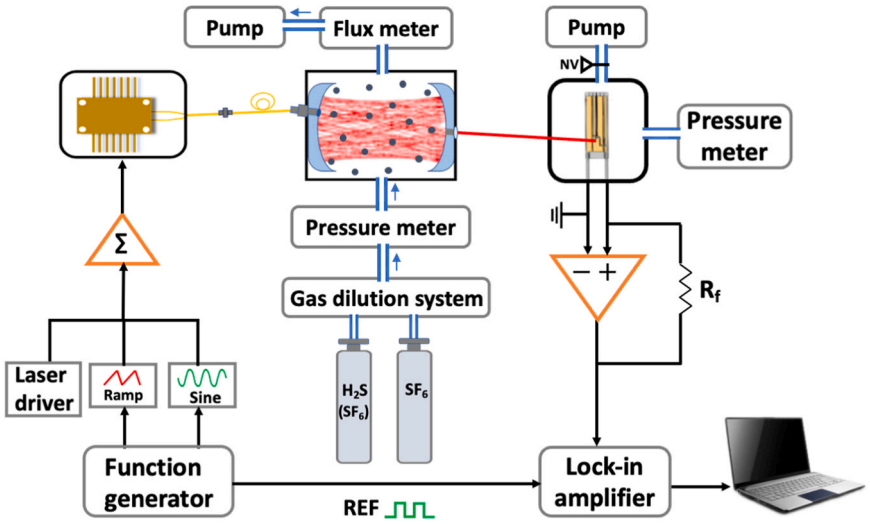

Fig. 3. Schematic of the LITES sensor for H_2S detection in the SF_6 matrix. NV: needle valve; Rf: feedback resistor.

significantly longer pathlength through multiple reflections of laser beam from the mirrors. The MMPC consists of two 1-inch CaF_2 spherical mirrors with a reflectivity of 99% and a radius of curvature of 2.5 cm. It is constructed with a cage structure measuring 6 cm × 4 cm × 4 cm, providing an internal sample volume of 67 cm^3. All brackets of the MMPC are made of carbon fiber material, which offers advantages such as high strain resistance, lightweight properties, and the ability to operate in extreme environments and ultra-high temperatures. The fiber collimator, equipped with a G-lens, is integrated on the left mirror frame (see Fig. 3). By utilizing the FC/APC interface, the fiber laser can be connected to the MMPC at an angle of 8° relative to the optical axis. Subsequently, the laser beam undergoes multiple reflections back and forth between the mirrors for a total of 107 times before eventually exiting through a small hole on the right mirror. A picture of the multi-pass cell light point/pattern is reported in Ref. [18]. Given the distance between the mirrors is ~3.9 cm, the total optical path length amounts to ~4.2 m.

4. System performance assessment

When the temperature of the laser driver is set to 31.3 °C and the output current to 148 mA, the wavenumber emission is 6320.55 cm^{-1} with an optical power of 30 mW. The function generator was utilized to enable periodic scanning of the 6320 cm^{-1} - 6321 cm^{-1} range by the laser, targeting the selected H_2S absorption line [43]. Since the performance of the LITES sensor operating in wavelength modulation depends on the current modulation amplitude, this parameter was preliminarily optimized. The peak-to-peak value of the current modulation maximizing the LITES signal was determined to be 19 mA. In the next step, the photodetection performance of the QTF was evaluated as a function of the operating pressure. As shown in Fig. 4, the WM LITES signal was measured for a gas mixture of 100 ppm H_2S/SF_6 at two different representative QTF pressures: 60 Torr and 5 Torr. The gas flow rate within the MMPC remained constant at 70 standard cubic centimeters per minute (sccm) for both measurements, while the pressure within the MMPC was maintained at atmospheric pressure (760 torr). It was observed that as the QTF pressure decreased, the LITES signal increased, reaching its highest value when operating at the lowest achievable pressure of 5 Torr. Under this condition, the LITES signal nearly doubled compared to the signal measured at 60 Torr. This behavior can be attributed to the fact that the LITES signal is proportional to the accumulation time of the oscillator, which is in turn related to the quality factor (Q-factor) of the QTF. The Q-factor is inversely proportional to the operating pressure. Based on this observation, all subsequent

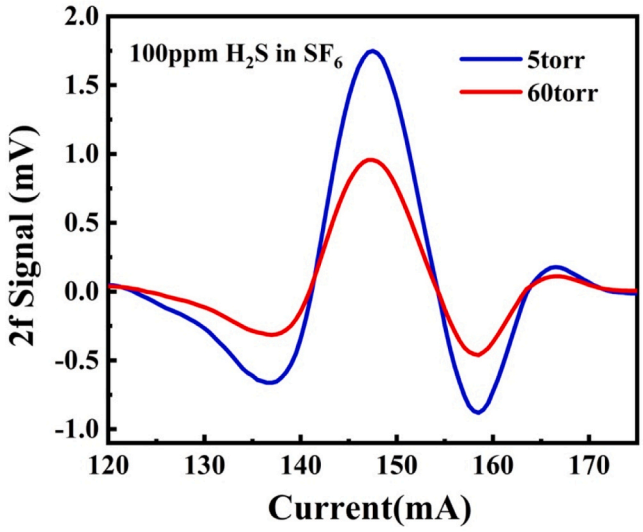

Fig. 4. Normalized WM LITES spectra measured for a mixture of 100 ppm H_2S in SF_6 at two different operating pressures of the QTF-photodetector: 5 Torr and 60 Torr.

experiments were conducted with the QTF operating at 5 Torr. The performance of the H_2S in SF_6 sensor system was then investigated.

Starting with the certified concentration of 100 ppm H2S in SF6, the LITES signal was measured at various H2S concentrations generated using a gas dilution system by keeping the flow rate always at 70 sccm. The spectral scans of the H_2S absorption line at different H_2S concentrations in SF_6 are reported in Fig. 5(a). For each spectral scan, the peak values were extracted and plotted as a function of H_2S concentrations in Fig. 5(b). The data were fitted with a linear function, yielding a slope of 21 μV/ppm and an R^2 value of 0.9996, indicating a highly linear sensor response to H_2S concentrations. The inset in Fig. 5(a) displays the background noise level of the system, measured in a spectral region with no H_2S absorption features. The 1-σ noise level was ~6 μV for an integration time of 300 ms and the minimum detection limit (MDL) of the sensor was ~300 ppb. The normalized noise equivalent absorption (NNEA) coefficient was determined to be 3.96 × 10^{-9} W·cm^{-1}·$Hz^{-1/2}$.

To estimate the 1σ-noise level as a function of the integration time, an Allan-Werle deviation analysis was conducted. During the analysis, the laser was locked onto the selected H_2S absorption peak while pure

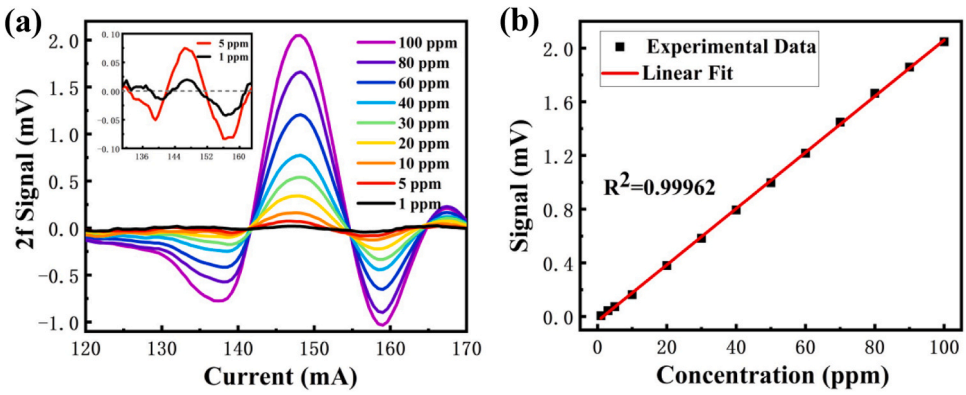

Fig. 5. (a) WM LITES spectra at different H_2S concentrations in SF_6, as reported. The laser current was swept from 120 mA to 170 mA. (b) QEPAS peak signals as a function of the H_2S concentrations, depicted by black square symbols. The data points were fitted with a linear function, shown by the red line, representing the best linear fit.

SF_6 was continuously flowing in the MMPC. The measured Allan-Werle deviation plot is shown in Fig. 6. Remarkably, a minimum detection limit of ~ 25 ppb can be achieved with an integration time of 100 s. This sensitivity level is achieved in half the time required by a recently reported multi-pass differential photoacoustic sensor, demonstrating the improved performance of our system [44].

For the real-time measurement of SF_6 decompositions in the GIS system, the response time is a crucial sensor parameter as it determines the accuracy of monitoring and plays a key role in timely maintenance of GIS equipment. A faster response time leads to reduced data delay distortion and enables early detection of GIS faults. The compact design of the enclosed MMPC, with an internal volume of only 67 cm^3, facilitates quick exchange of the gas sample, allowing for real-time measurement of H_2S concentration. To evaluate the sensor's response time, a gas flow rate of 70 sccm was chosen, and initially, pure SF_6 was purged inside the MMPC. The laser drive current was set at 148 mA to lock the laser wavelength to the peak of the H_2S absorption line. Subsequently, a rapid switching mechanism interrupted the flow of pure SF_6 and initiated the flow of a 100 ppm H_2S in SF_6 mixture into the MMPC. The rise time refers to the duration required for the LITES signal to increase from the background level to its steady-state value. Finally, the system was switched back to pure SF_6 to measure the fall time, which represents the duration needed to reach the background signal level. Fig. 7 depicts that

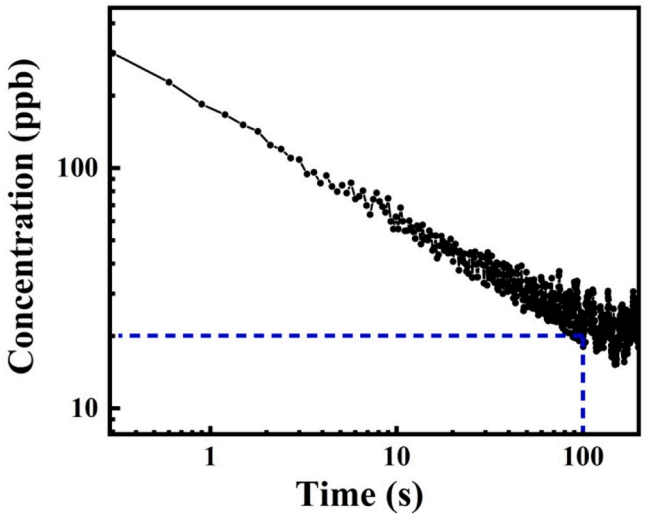

Fig. 6. Allan-Werle deviation plot of the QEPAS signal measured in pure SF_6 as a function of the integration time. For a 100 s integration time, the minimum detection limit can be significantly reduced to ~25 ppb.

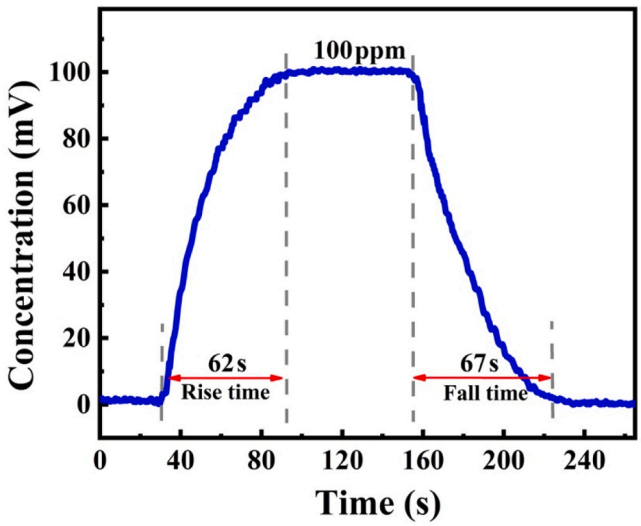

Fig. 7. Sensor response time measurement. Rise and fall times are highlighted in the graph.

the recorded sensor signal during all the measurements. The rise time and fall time were determined to be ~62 s and ~67 s respectively, which aligns well with the estimated MMPC sample exchange time of ~57 s (chamber volume divided by gas flow rate). The test was repeated multiple times without any discernible differences.

5. Conclusions

In this work, we reported on a LITES sensor capable of detecting H_2S concentrations in a SF_6 matrix. LITES, as a non-contact sensing technique, is well-suited for applications that involve the analysis of corrosive gas samples, such as decomposed SF_6 matrices. The sensor setup consisted of a 1.58 μm DFB laser as the excitation source and a standard QTF coupled with a compact multi-pass cell as the photodetector. The sensor exhibited a linear dynamic range of 0–100 ppm, with an achieved MDL of ~300 ppb and an integration time of 300 ms. This sensitivity improved to ~25 ppb for a longer integration time of 100 s. The sensor demonstrated a response time of ~1 min for a gas flow rate of 70 sccm. These achieved performance metrics meet the requirements for monitoring GIS systems. In future developments, erbium-doped fiber amplifiers could be implemented to enhance the laser power and further improve the detection sensitivity.

Declaration of Competing Interest

The authors declare that they have no known competing financial interests or personal relationships that could have appeared to influence the work reported in this paper.

Data Availability

Data will be made available on request.

Acknowledgements

The project is supported by National Key Research and Development Program of China [grant nunmber 2019YFE0118200); National Natural Science Foundation of China (NSFC) [grant nunmbers 62235010, 62175137, 62122045, 62075119]; The Shanxi Science Fund for Distinguished Young Scholars (20210302121003). Bo Sun acknowledges financial support from the program of China Scholarship Council (No. 202208140093).

References

[1] X. Li, H. Zhao, A.B. Murphy, SF_6-alternative gases for application in gas-insulated switchgear, J. Phys. D. Appl. Phys. 51 (15) (2018), 153001.
[2] X. Zhang, E. Gockenbach, Z. Liu, H. Chen, L. Yang, Reliability estimation of high voltage SF_6 circuit breakers by statistical analysis on the basis of the field data, Electri. Pow. Syst. Res. 103 (2013) 105–113.
[3] J. Zhou, W. Chen, H. Tu, L. Wang, H. Ni, Study on the application of 220/20kV SF_6 gas transformer, Front. Mech. Eng. -prc. 2 (1) (2020) 5–8.
[4] R. Hu, X. Cui, W. Chen, Z. Sun, L. Qi, W. Zhang, Z. Li, M. Dai, Simulation of very fast transient overvoltage on UHV 1000kV GIS test circuit, Sixth International Conference on Electromagnetic Field Problems and Applications (2012), 1–4.
[5] W. Gao, D. Ding, W. Liu, X. Huang, Analysis of the intrinsic characteristics of the partial discharge induced by typical defects in GIS, Ieee. T. Dielect. El. 20 (3) (2013).
[6] A.S. Mahdi, Z.A. Malek, R.N. Arshad, SF_6 decomposed component analysis for partial discharge diagnosis in GIS: A Review, Ieee Access 10 (2022) 27270–27288.
[7] B. Li, Q. Zhou, R. Peng, Y. Liao, W. Zeng, Adsorption of SF_6 decomposition gases (H_2S, SO_2, SOF_2 and SO_2F_2) on Sc-doped MoS_2 surface: A DFT study, Appl. Surf. Sci. 549 (30) (2021), 149271.
[8] N.S. Shuman, T.M. Miller, N. Hazari, E.D. Luzik Jr., A.A. Viggiano, Kinetics following addition of sulfur fluorides to a weakly ionized plasma from 300 to 500 K: Rate constants and product determinations for ion–ion mutual neutralization and thermal electron attachment to SF_5, SF_3, and SF_2, J. Chem. Phys. 133 (23) (2010), 234304.
[9] F. Zeng, J. Tang, X. Zhang, H. Sun, Q. Yao, Y. Miao, Study on the influence mechanism of trace H_2O on SF_6 thermal decomposition characteristic components, Ieee. T. Dielect. El. 22 (2) (2015) 766–774.
[10] H. Huang, Y. Yu, M. Zhang, Analysis of adsorption properties of SF_6 decomposed gases (SOF_2, SO_2F_2, SF_4, CF_4, and HF) on Fe-doped SWCNT: a DFT study, Appl. Surf. Sci. 505 (1) (2020), 144622.
[11] R. Cui, L. Dong, H. Wu, S. Li, L. Zhang, W. Ma, W. Yin, L. Xiao, S. Jia, F.K. Tittel, Highly sensitive and selective CO sensor using a 2.33 μm diode laser and wavelength modulation spectroscopy, Opt. Express 26 (19) (2018) 24318–24328.
[12] H. Dai, P. Xiao, Qi Lou, Application of SnO_2/MWCNTs nanocomposite for SF_6 decomposition gas sensor, Phys. Status Solidi A 208 (7) (2011) 1714–1717.
[13] X. Yin, L. Dong, H. Wu, W. Ma, L. Zhang, W. Yin, L. Xiao, S. Jia, F.K. Tittel, Ppb-level H_2S detection for SF_6 decomposition based on a fiber-amplified telecommunication diode laser and a background-gas-induced high-Q photoacoustic cell, Appl. Phys. Lett. 111 (3) (2017), 031109.
[14] H. Liu, Q. Zhou, Q. Zhang, C. Hong, L. Xu, L. Jin, W. Chen, Synthesis, Characterization and enhanced sensing properties of a NiO/ZnO p–n junctions sensor for the SF_6 decomposition byproducts SO_2, SO_2F_2, and SOF_2, Sens. (Basel). 17 (2017) 913.
[15] O. Kóréh, T. Rikker, G. Molnár, B.M. Mahara, K. Torkos, J. Borossay, Study of decomposition of sulphur hexafluoride by gas chromatography/mass spectrometry, Rapid. Commun. Mass. Sp. 11 (15) (1998) 1643–1648.
[16] A.M. Casanovas, J. Casanovas, F. Lagarde, A. Belarbi, Study of the decomposition of SF_6 under dc negative polarity corona discharges (point to plane geometry): influence of the metal constituting the plane electrode, J. Appl. Phys. 72 (8) (1992) 3344.
[17] X. Yin, H. Wu, L. Dong, W. Ma, L. Zhang, W. Yin, L. Xiao, S. Jia, F.K. Tittel, Ppb-level photoacoustic sensor system for saturation-free CO detection of SF_6 decomposition by use of a 10 W fiber-amplified near-infrared diode laser, Sens. Actuat. B-Chem. 282 (2019) 567–573.
[18] R. Cui, L. Dong, H. Wu, W. Ma, L. Xiao, S. Jia, W. Chen, F.K. Tittel, Three-dimensional printed miniature fiber-coupled multipass cells with dense spot patterns for ppb-level methane detection using a near-IR diode laser, Anal. Chem. 92 (2020) 13034–13041.
[19] A.A. Kosterev, Y.A. Bakhirkin, R.F. Curl, F.K. Tittel, Quartz-enhanced photoacoustic spectroscopy, Opt. Lett. 27 (21) (2002) 1902–1904.
[20] B. Sun, A. Zifarelli, H. Wu, S.D. Russo, S. Li, P. Patimisco, L. Dong, V. Spagnolo, Mid-infrared quartz-enhanced photoacoustic sensor for ppb-level CO detection in a SF_6 gas matrix exploiting a T-Grooved quartz tuning fork, Anal. Chem. 92 (20) (2020) 13922–13929.
[21] A. Sil, V.N. Kumar, Comprehensive empirical equation for assessing atmospheric corrosion progression of Steel considering environmental parameters, Corros. Sci. Technol. 19 (4) (2020) 174–188.
[22] A. Kahyarian, S. Nesic, H_2S corrosion of mild steel: a quantitative analysis of the mechanism of the cathodic reaction, Electrochim. Acta 297 (2019) 676–684.
[23] Q. Wu, H. Lv, J. Li, Z. Yang, R. Kan, M. Giglio, W. Zhu, Y. Zhong, A. Sampaolo, P. Patimisco, V. Spagnolo, J. Yu, H. Zheng, Side-excitation light-induced thermoelastic spectroscopy, Opt. Lett. 48 (3) (2023) 562–565.
[24] Y. He, Y. Ma, Y. Tong, X. Yu, F.K. Tittel, Ultra-high sensitive light-induced thermoelastic spectroscopy sensor with a high Q-factor quartz tuning fork and a multipass cell, Opt. Lett. 44 (8) (2019) 1904–1907.
[25] Y. Ma, Y. He, Y. Tong, X. Yu, F.K. Tittel, Quartz-tuning-fork enhanced photothermal spectroscopy for ultra-high sensitive trace gas detection, Opt. Express 26 (24) (2018) 32103–32110.
[26] Y. Ma, T. Liang, S. Qiao, X. Liu, Z. Lang, Highly sensitive and fast hydrogen detection based on light-induced thermoelastic spectroscopy, Ultra Sci. 3 (2023) 0024.
[27] Z. Lang, S. Qiao, Y. Ma, Fabry–Perot-based phase demodulation of heterodyne light-induced thermoelastic spectroscopy, Light.: Adv. Manuf. 4 (2023) 23.
[28] Y. Pan, J. Zhao, P. Lu, C. Sima, W. Zhang, L. Fu, D. Liu, J. Zhang, H. Wu, L. Dong, All-optical light-induced thermoacoustic spectroscopy for remote and non-contact gas sensing, Photoacoustics 27 (2022), 100389.
[29] Y. Pan, J. Zhao, P. Lu, C. Sima, D. Liu, Recent advances in light-induced thermoelastic spectroscopy for gas sensing: a review, Remote Sens-basel 15 (2023) 69.
[30] S.D. Russo, A. Zifarelli, P. Patimisco, A. Sampaolo, T. Wei, H. Wu, L. Dong, V. Spagnolo, Light-induced thermo-elastic effect in quartz tuning forks exploited as a photodetector in gas absorption spectroscopy, Opt. Express 28 (2020) 19074–19084.
[31] M. Olivieri, A. Zifarelli, G. Menduni, M.D. Gioia, C. Marzocca, V.M.N. Passaro, A. Sampaolo, M. Giglio, Vi Spagnolo, P. Patimisco, Influence of air pressure on the resonance properties of a T-shaped quartz tuning fork coupled with resonator tubes, Appl. Sci. -basel 11 (17) (2021) 7974.
[32] P. Patimisco, A. Sampaolo, M. Giglio, S.D. Russo, V. Mackowiak, H. Rossmadl, A. Cable, F.K. Tittel, V. Spagnolo, Tuning forks with optimized geometries for quartz-enhanced photoacoustic spectroscopy, Opt. Express 27 (2) (2019) 1401–1415.
[33] S.D. Russo, A. Sampaolo, P. Patimisco, M. Giansergio, M. Giglio, C. Hoelzl, V.M. N. Passaro, H. Wu, L. Dong, V. Spagnolo, Quartz-enhanced photoacoustic spectroscopy exploiting low-frequency tuning forks as a tool to measure the vibrational relaxation rate in gas species, Photoacoustics 21 (2021), 100227.
[34] P. Patimisco, G. Scamarcio, F.K. Tittel, V. Spagnolo, Quartz-enhanced photoacoustic spectroscopy: a review, Sens. (Basel). 14 (2014) 6165–6206.
[35] P. Patimisco, A. Sampaolo, L. Dong, F.K. Tittel, V. Spagnolo, Recent advances in quartz enhanced photoacoustic sensing, Appl. Phys. Rev. 5 (1) (2018), 011106.
[36] A.A. Kosterev, P.R. Buerki, L. Dong, M.L. Reed, T. Day, F.K. Tittel, QEPAS detector for rapid spectral measureme, Appl. Phys. B-Lasers O. 100 (2010) 173–180.
[37] A. Sampaolo, P. Patimisco, M. Giglio, A. Zifarelli, H. Wu, L. Dong, V. Spagnolo, Quartz-enhanced photoacoustic spectroscopy for multi-gas detection: a review, Anal. Chim. Acta 1202 (2022), 338894.
[38] H. Hosaka, K. Itao, S. Kuroda, Damping characteristics of beam-shaped micro-oscillators, Sens. Actuat. A-Phys. 49 (1995) 87–95.
[39] T. Wei, H. Wu, L. Dong, R. Cui, S. Jia, Palm-sized methane TDLAS sensor based on a mini-multi-pass cell and a quartz tuning fork as a thermal detector, Opt. Express 29 (8) (2021) 12357–12364.
[40] T. Wei, A. Zifarelli, S.D. Russo, H. Wu, G. Menduni, P. Patimisco, A. Sampaolo, V. Spagnolo, L. Dong, High and flat spectral responsivity of quartz tuning fork used as infrared photodetector in tunable diode laser spectroscopy, Appl. Phys. Rev. 8 (4) (2021), 041409.
[41] Y. Ma, Y. He, P. Patimisco, A. Sampaolo, S. Qiao, X. Yu, F.K. Tittel, V. Spagnolo, Ultra-high sensitive trace gas detection based on light-induced thermoelastic spectroscopy and a custom quartz tuning fork, Appl. Phys. Lett. 116 (2020), 011103.
[42] Y. Ma, Recent advances in QEPAS and QEPTS based trace gas sensing: a review, Front Phys. -Lausanne 8 (2020) 268.
[43] C. Feng, M. Giglio, B. Li, A. Sampaolo, P. Patimisco, V. Spagnolo, L. Dong, H. Wu, Detection of hydrogen sulfide in sewer using an erbium-doped fiber amplified diode laser and a gold-plated photoacoustic cell, Molecules 27 (2022) 6505.
[44] X. Zhao, M. Guo, D. Cui, C. Li, H. Qi, K. Chen, F. Ma, J. Huang, G. Zhang, J. Zhao, Multi-pass differential photoacoustic sensor for real-time measurement of SF_6 decomposition component H_2S at the ppb Level, Anal. Chem. (2023), https://doi.org/10.1021/acs.analchem.3c00003.

Bo Sun is now pursuing a double Ph.D. degree in the Institute of Laser Spectroscopy of Shanxi university, China and Department of Electrical and Information Engineering of Politecnico di Bari, Italy. The majors are "atomic and molecular physics" and "industrial research 4.0" respectively. Her research interests include photoacoustic spectroscopy, light-induced thermoelastic spectroscopy and optical sensor.

Pietro Patimisco obtained the Master degree in Physics (cum laude) in 2009 and the PhD Degree in Physics in 2013 from the University of Bari. Since 2018, he is Assistant professor at the Technical University of Bari. Dr. Patimisco's scientific activity addressed the study and applications of trace-gas sensors, such as quartz-enhanced photoacoustic spectroscopy and cavity enhanced absorption spectroscopy in the mid infrared and terahertz spectral region, leading to several publications.

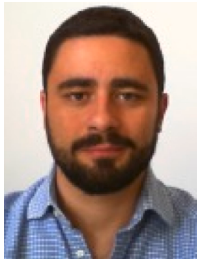

Angelo Sampaolo obtained his Master degree in Physics in 2013 and the PhD Degree in Physics in 2017 from University of Bari. He was an associate researcher in the Laser Science Group at Rice University from 2014 to 2016 and associate researcher at Shanxi University since 2018. Since 2019, he is Assistant Professor at Polytechnic of Bari. His research activity has focused on the development of innovative techniques in trace gas sensing, based on Quartz-Enhanced Photoacoustic Spectroscopy and covering the full spectral range from near-IR to THz.

Andrea Zifarelli obtained his M.S. degree (cum laude) in Physics in 2018 from the University of Bari. From the same year, he is a PhD student at the Physics Department of the University of Bari, developing his research work at PolySense Lab, joint-research laboratory between Technical University of Bari and THORLABS GmbH. Currently, his research activities are focused on the development of gas sensors based on Quartz-Enhanced Photoacoustic Spectroscopy for detection of gas mixtures and broadband absorbers, exploiting non-conventional laser sources.

Vincenzo Spagnolo received the degree (summa cum laude) and the PhD, both in physics, from University of Bari. He works as Full Professor of Applied Physics at the Technical University of Bari. In 2019, he become Vice-Rector of the Technical University of Bari, deputy to Technology Transfer. Since 2017, he is the director of the joint-research lab PolySense, created by THORLABS GmbH and Technical University of Bari, devoted to the development and implementation of novel gas sensing techniques and the realization of highly sensitive QEPAS trace-gas sensors.

Hongpeng Wu received his Ph.D. degree in atomic and molecular physics from Shanxi University, China, in 2017. From September, 2015 to October, 2016, he studied as a joint Ph.D. student in the Electrical and Computer Engineering Department and Rice Quantum Institute, Rice University, Houston, USA. Currently he is a professor in the Institute of Laser Spectroscopy of Shanxi University. His research interests include gas sensors, photoacoustic spectroscopy, photothermal spectroscope and laser spectroscopy techniques.

Lei Dong received his Ph.D. degree in optics from Shanxi University, China, in 2007. From June, 2008 to December, 2011, he worked as a post-doctoral fellow in the Electrical and Computer Engineering Department and Rice Quantum Institute, Rice University, Houston, USA. Currently he is a professor in the Institute of Laser Spectroscopy of Shanxi University. His research interests include optical sensors, trace gas detection, photoacoustic spectroscopy and laser spectroscopy.